

Stable single layer of Janus MoSO: Strong out-of-plane piezoelectricity

M. Yagmurcukardes* and F. M. Peeters

Department of Physics, University of Antwerp, Groenenborgerlaan 171, B-2020 Antwerp, Belgium

(Received 11 January 2020; revised manuscript received 22 March 2020; accepted 27 March 2020; published 24 April 2020)

Using density functional theory based first-principles calculations, we predict the dynamically stable 1H phase of a Janus single layer composed of S-Mo-O atomic layers. It is an indirect band gap semiconductor exhibiting strong polarization arising from the charge difference on the two surfaces. In contrast to 1H phases of MoS₂ and MoO₂, Janus MoSO is found to possess four Raman active phonon modes and a large out-of-plane piezoelectric coefficient which is absent in fully symmetric single layers of MoS₂ and MoO₂. We investigated the electronic and phononic properties under applied biaxial strain and found an electronic phase transition with tensile strain while the conduction band edge displays a shift when under compressive strain. Furthermore, single-layer MoSO exhibits phononic stability up to 5% of compressive and 11% of tensile strain with significant phonon shifts. The phonon instability is shown to arise from the soft in-plane and out-of-plane acoustic modes at finite wave vector. The large strain tolerance of Janus MoSO is important for nanoelastic applications. In view of the dynamical stability even under moderate strain, we expect that Janus MoSO can be fabricated in the common 1H phase with a strong out-of-plane piezoelectric coefficient.

DOI: [10.1103/PhysRevB.101.155205](https://doi.org/10.1103/PhysRevB.101.155205)**I. INTRODUCTION**

The successful exfoliation of graphene [1] has opened an exponentially growing research field of two-dimensional (2D) ultrathin materials. Among the 2D ultrathin materials, transition metal dichalcogenides (TMDs) have gained a lot of attention owing to their potential for applications in, e.g., optoelectronic devices [2–6].

Single-layer MoS₂ has been extensively investigated both experimentally and theoretically because of its distinctive electronic, optical, and mechanical properties [7–12]. The direct band gap nature of 1H-MoS₂ has made it a suitable candidate for applications in photonics. Previous experiments have demonstrated that, to synthesize MoS₂ by chemical vapor deposition (CVD), MoO₃ could be used as the Mo precursor [13–15]. In addition, it has also been demonstrated that incomplete sulfurization of MoO₃ leads to the formation of either molybdenum oxides, MoO_{3–x}, or molybdenum oxysulfides, MoO_{3–x}S_y [16–19]. Therefore, the formation of a fully asymmetric MoSO structure can be feasible in such experiments. The question is whether the structural phase of such fully asymmetric MoSO can be controlled or not.

On the other hand, recent experimental techniques have allowed successful replacement of one Se layer of MoSe₂ by S atoms and construction of a polar single layer, namely Janus MoSSe [20,21]. The induced internal out-of-plane polarization opens up a way to tune the properties of 2D ultrathin materials. Following the experimental realization of Janus MoSSe, out-of-plane asymmetric single layers of various TMDs and other 2D materials have been theoretically proposed [22–26]. The experimentally realized single-layer

MoSSe was constructed by replacing one surface of single-layer MoX₂ by a different chalcogen atom in a common structural phase, namely 1H phase. Similar to the formation process of Janus MoSSe, the synthesis of single-layer MoS₂ from MoO₃ powders motivated us to predict a possible new 1H phase of Janus MoSO composed of S-Mo-O atomic layers. Alternatively, since the formation of molybdenum oxysulfides, MoO_{3–x}S_y, has been observed in previous experiments, it may also be feasible to construct a Janus single layer in such an experiment as an intermediate state.

In this study, we show that the formation of a Janus single layer, composed of S and O layers on different surfaces, leads to the dynamically stable 1H-MoSO, which is an indirect band gap semiconductor. We show that the formation of Janus MoSO can be distinguished by its Raman spectrum in which the broken out-of-plane symmetry creates additional Raman active phonon modes. In addition, it is shown that Janus MoSO exhibits a large out-of-plane piezoelectric coefficient due to the significant charge difference between the two surfaces. Moreover, we investigate the effect of an external biaxial strain on the electronic and phononic properties of single-layer MoSO. Our results indicate that Janus MoSO can withstand large tensile strains and displays a semiconductor-to-metal transition with tensile strain.

II. COMPUTATIONAL METHODOLOGY

The plane-wave basis projector augmented wave (PAW) method was employed in the framework of density-functional theory (DFT) in our first-principles calculations. The generalized gradient approximation (GGA) in the Perdew-Burke-Ernzerhof (PBE) form [27,28] was used for the exchange-correlation potential as implemented in the Vienna *ab initio* Simulation Package (VASP) [29,30]. For the electronic-band

*Mehmet.Yagmurcukardes@uantwerpen.be

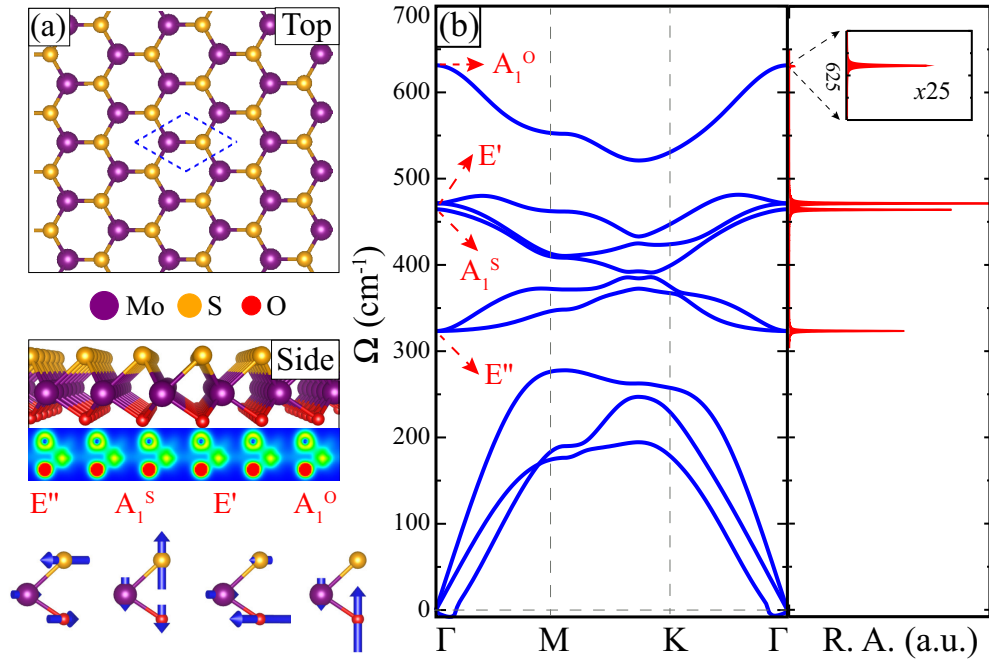


FIG. 1. Single layer of Janus MoSO crystal. (a) Top and side views of the structure and increasing charge density is shown by a color scheme from blue to red with linear scaling between zero (blue) and $6.9 e/\text{\AA}^3$ (red). The unit cell is indicated by the blue dashed parallelogram. In addition, the motions of the atoms for the four Raman active modes are shown (bottom). (b) The phonon band dispersions with corresponding Raman spectrum (right panel).

structure calculations spin-orbit coupling (SOC) was included with the GGA functional and Heyd-Scuseria-Ernzerhof (HSE06) screened-nonlocal-exchange functional of the generalized Kohn-Sham scheme [31]. The van der Waals correction to the GGA functional was included by using the DFT-D2 method of Grimme [32]. Analysis of the charge transfers in the structure was determined by the Bader technique [33].

The kinetic energy cutoff for the plane-wave expansion was set to 500 eV and the energy was minimized until its variation became less than 10^{-8} eV during the electronic and structural optimizations. The Gaussian smearing method was employed for the total energy calculations and the width of the smearing was chosen as 0.05 eV. Total Hellmann-Feynman force was reduced to 10^{-7} eV/ \AA for the structural optimization. $24 \times 24 \times 1$ Γ centered k -point samplings were used for the primitive unit cells. To avoid interaction between the neighboring layers, a vacuum space of 25 \AA was implemented in the calculations.

Phonon band dispersions were calculated by using the small displacement method as implemented in the PHON code [34] by considering a $5 \times 5 \times 1$ supercell. Each atom in the primitive unit cell was initially distorted by 0.01 \AA and the corresponding dynamical matrix was constructed. Then, the vibrational modes were determined by a direct diagonalization of the dynamical matrix. The corresponding Raman activity of each phonon mode was obtained from the derivative of the macroscopic dielectric tensor by using the finite-difference method. The relaxed-ion elastic stiffness tensors are calculated by using the small displacement methodology as implemented in VASP. In addition, the piezoelectric stress coefficients are obtained directly using density functional perturbation theory (DFPT) with a sufficiently large k -point

sampling and kinetic energy cutoff of 700 eV. Moreover, the thermal stability of single-layer Janus MoSO is examined such that for the simulations the NVE ensemble is used with a $4 \times 4 \times 1$ supercell. The temperature is increased from 0 to 1000 K in 10 ps with 2 fs between consequent steps (see Fig. S2 in the Supplemental Material [35]).

III. SINGLE-LAYER JANUS MoSO

The optimized crystal structure of single-layer Janus MoSO possessing the 1H crystal phase is shown in Fig. 1(a). Note that the 1T phase of Janus MoSO is dynamically unstable (see Fig. S3 in the Supplemental Material [35]). As shown in the figure, the Janus structure is constructed such that the atomic layer of molybdenum (Mo) is antisymmetrically sandwiched between the atomic layers of sulfur (S) and oxygen (O). The optimized in-plane lattice constant of single-layer MoSO is $a = b = 3.00$ \AA . Since the lattice constants of single-layer MoS₂ (MoO₂) are larger (smaller) than those of the Janus structure (see Table I), compressive (tensile) strains on S (6.0%) and O (6.4%) surfaces, occurs. The Mo-S and Mo-O bond lengths are 2.38 and 2.09 \AA , respectively, which are slightly different from those in MoS₂ and MoO₂ due to the induced surface strains. Bader charge analysis reveals that the charge transfer from a Mo atom to the chalcogenide atoms is different: 0.5 and 0.9 e charges are donated to S and O atoms, respectively, which results in a strong out-of-plane polarization. Moreover, the charge difference on the surfaces affects also the anisotropy of the work function, Φ , as listed in Table I.

The dynamical stability of single-layer Janus MoSO is verified by calculating its phonon band dispersions through the

TABLE I. For the single-layer crystals of MoS₂, MoO₂, and Janus MoSO we give the optimized lattice constants, a and b ; atomic bond lengths in the crystal, $d_{\text{Mo-S}}$ and $d_{\text{Mo-O}}$; the amounts of charge depletion, $\Delta_{\rho(\text{Mo-S})}$ and $\Delta_{\rho(\text{Mo-O})}$; energy band gaps calculated within SOC on top of GGA, $E_{\text{gap}}^{\text{GGA}}$ and HSE on top of GGA+SOC, $E_{\text{gap}}^{\text{HSE06}}$; the work functions calculated for two different surfaces, Φ_O and Φ_S ; and locations of VBM and CBM edges in the BZ.

| | a (Å) | b (Å) | $d_{\text{Mo-S}}$ (Å) | $d_{\text{Mo-O}}$ (Å) | $\Delta_{\rho(\text{Mo-S})}$ (e) | $\Delta_{\rho(\text{Mo-O})}$ (e) | $E_{\text{gap}}^{\text{GGA}}$ (eV) | $E_{\text{gap}}^{\text{HSE06}}$ (eV) | Φ_O (eV) | Φ_S (eV) | VBM/CBM |
|------------------|------------|------------|--------------------------|--------------------------|-------------------------------------|-------------------------------------|---------------------------------------|---|------------------|------------------|------------|
| MoS ₂ | 3.19 | 3.19 | 2.41 | | 0.6 | | 1.04 | 1.98 | | 5.70 | K/K |
| MoO ₂ | 2.82 | 2.82 | | 2.05 | | 0.8 | 0.97 | 1.56 | 6.52 | | Γ/K |
| MoSO | 3.00 | 3.00 | 2.38 | 2.09 | 0.5 | 0.9 | 1.07 | 1.62 | 6.63 | 4.67 | Γ/K |

whole BZ, which is presented in Fig. 1(b). As shown, phonon branches are almost free from any imaginary frequencies, except around the Γ point, indicating the dynamical stability of the structure. Small imaginary frequencies in the out-of-plane acoustic mode near the Γ point arise from numerical artifacts caused by the inaccuracy of the fast Fourier transform (FFT) grid. In its three-atom primitive unit cell, single-layer MoSO exhibits six optical phonon branches. As shown in the bottom panel of Fig. 1(a), there are two doubly degenerate in-plane modes, namely E' and E'' , and two nondegenerate out-of-plane vibrational modes, denoted by A_1^O and A_1^S . The calculated Raman spectrum of single-layer MoSO reveals that all six optical phonon modes are Raman active. In a symmetric 1H-phase single-layer TMD, it is known that there are two doubly degenerate and one nondegenerate Raman active modes. However, in the Janus structure there is an additional Raman active mode arising from the broken out-of-plane symmetry. Except for the A_1^O mode, all three atoms contribute to the vibration of the other optical phonon modes. The A_1^O mode arises from out-of-plane vibration of Mo and O atoms against each other. Its relatively high frequency (631.3 cm⁻¹ at the Γ point) originates from strong Mo-O bond stretching. The other out-of-plane mode, A_1^S , denotes the opposite vibration of the S and Mo-O pair and the vibration is dominated by the S atom. The frequency of A_1^S is calculated to be 464.3 cm⁻¹ which is slightly larger than that of A_{2u} in single-layer MoS₂ (461.5 cm⁻¹).

The in-plane phonon modes can be classified as E' , which is dominated by the O vibration, and E'' is dominated by the S vibration. The E' mode has a frequency of 471.5 cm⁻¹ and it is attributed to the opposite vibrations of Mo-O atoms against each other. On the other hand, the E'' mode has a much lower frequency, 323.4 cm⁻¹, and the phonon mode arises from the in-plane opposite vibrations of S and Mo-O pairs. Both modes are found to be Raman active and the calculated Raman activity of E' is found to be larger than that of E'' . Note that in a symmetric single-layer TMD, the E'' phonon mode arises from the opposite vibration of the chalcogen atoms while the transition-metal atom has no contribution to the vibration. Moreover, its Raman activity is almost three to four orders of magnitude smaller than those of the other phonon modes.

The electronic properties of single-layer MoSO reveal many more distinctive properties than the fully symmetric single layers of MoS₂ and MoO₂ due to the different bonding states of Mo-S and Mo-O atoms. The atomic contributions to the electronic band dispersions of Janus MoSO are investigated through the whole BZ and are presented in

Figs. 2(a), 2(b), and 2(c). As in the case of the single-layers MoS₂ and MoO₂, Janus MoSO exhibits semiconducting behavior with a band gap of 1.62 eV calculated with the HSE06 functional. In contrast to the direct band gap semiconducting nature of single-layer MoS₂, whose conduction band minimum (CBM) and valence band maximum (VBM) reside at the K point, MoO₂ is an indirect band gap semiconductor with its CBM and VBM residing at the K and the Γ points, respectively (see Fig. S1 in the Supplemental Material [35]). As shown in Fig. 2(c), the VBM of Janus MoSO is composed of orbitals hybridized between d -Mo and p_z -O atoms. However, as in the case of single-layer MoS₂ and MoO₂, the CBM is dominated by the Mo orbitals only. The domination of VBM by the Mo-O bonding states results in the indirect band gap behavior of Janus MoSO.

The piezoelectric effect is known to generate an electric dipole moment as a result of applied mechanical stress in noncentrosymmetric materials. Theoretical predictions and experimental observations have demonstrated that in the 2D limit the piezoelectric constants of materials can be enhanced [36–39].

The relaxed-ion piezoelectric tensor e_{ij} can be described as the sum of ionic, e_{ij}^{ion} , and electronic, e_{ij}^{el} , contributions. The piezoelectric stress tensor e_{ij} then is related to the piezoelectric strain tensor d_{ij} through the elastic stiffness tensor C_{ij} as follows:

$$e_{ij} = d_{ik}C_{kj}. \quad (1)$$

As already reported before, for structures exhibiting hexagonal symmetry, the piezoelectric strain coefficients can be found by using the relations

$$d_{11} = \frac{e_{11}}{C_{11} - C_{12}}, \quad d_{13} = \frac{e_{13}}{C_{11} + C_{12}}. \quad (2)$$

Note that for the out-of-plane symmetric single layers the coefficient d_{31} does not exist; however, in the presence of surface chalcogen replacement, i.e., in Janus single layers, out-of-plane piezoelectricity is created. As listed in Table II, the single layers of MoS₂ and MoO₂ have an in-plane piezoelectric property while the replacement of S by O on one surface creates a considerably strong out-of-plane piezoelectricity. For comparison, we also calculated the piezoelectric constants for experimentally synthesized MoSSe and other predicted single-layer Janus TMDs. The e_{11} component is found to be 3.7×10^{-10} C/m for single-layer MoSO, which is close to that of single-layer MoS₂ and MoSSe. The breaking of out-of-plane symmetry adds an additional degree of freedom and

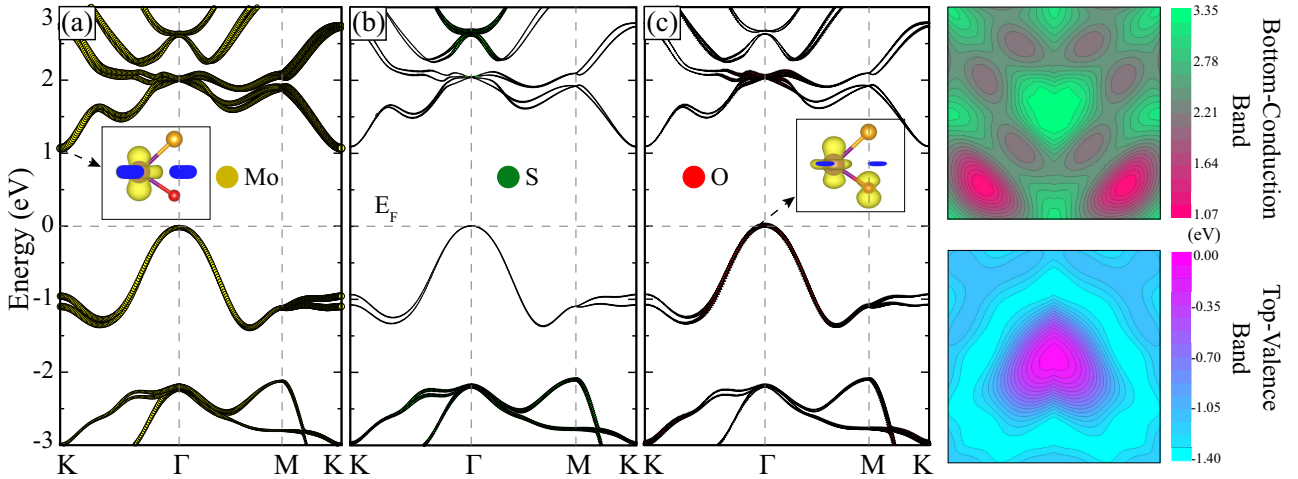


FIG. 2. The atomic contributions to the electronic band dispersions of Janus MoSO with (a) Mo, (b) S, and (c) O contributions. Energy surfaces of the valence and conduction band edges are shown in the right panel. The insets show the atomic orbital characters of the valence and the conduction band edges. The Fermi level is set to zero energy.

d_{13} is no longer zero. As shown in Fig. 3, the e_{31} coefficient for MoSO is found to be 1.4×10^{-10} C/m, which is much larger than for the other predicted Janus TMDs. The relatively larger charge difference between two surfaces of Janus MoSO results in a large out-of-plane polarization and thus the e_{31} and the corresponding d_{31} coefficients are found to be large in Janus MoSO.

IV. BIAXIAL STRAINED SMOO

Strain is often present in experiments either naturally or controllably. Many reports indicated that strain can alter the electronic and the vibrational properties of materials [40,41]. In the case of the vibrational spectrum, Raman peak positions and the corresponding intensities depend significantly on the presence of strain [42,43]. In addition, strain modifies the phonons, with stretching usually resulting in phonon mode softening, and phonon hardening in the case of compression. The rate of change can be obtained from the Grüneisen parameter. Moreover, by the presence of strain, the relative Raman intensities can be more distinguishable.

TABLE II. For the 1H phases of single-layer MoS₂, MoO₂, and MoSO, the relaxed-ion elastic coefficients C_{ij} , piezoelectric stress coefficients e_{ij} , and the corresponding piezoelectric strain coefficients d_{ij} . Note that e_{ij} is multiplied by 10^{-10} .

| | C_{11} (N/m) | C_{12} (N/m) | e_{11} (C/m) | e_{13} (C/m) | d_{11} (pm/V) | d_{13} (pm/V) |
|------------------|-------------------|-------------------|-------------------|-------------------|--------------------|--------------------|
| MoS ₂ | 131 | 34 | 3.7 | | 3.8 | |
| MoO ₂ | 229 | 84 | 3.5 | | 2.4 | |
| MoSO | 164 | 48 | 3.7 | 1.4 | 3.2 | 0.7 |
| SMoSe | 135 | 30 | 3.8 | 0.3 | 3.7 | 0.2 |
| SMoTe | 116 | 28 | 4.5 | 0.5 | 5.1 | 0.4 |
| SeMoTe | 110 | 23 | 4.5 | 0.2 | 5.2 | 0.2 |
| SWSe | 147 | 28 | 2.6 | 0.2 | 2.2 | 0.1 |
| SWTe | 131 | 22 | 3.2 | 0.4 | 3.0 | 0.2 |
| SeWTe | 119 | 19 | 3.2 | 0.2 | 3.2 | 0.1 |

A. Electronic structure

In our work, we extend the applied biaxial strain to the nonlinear regime in order to investigate also the phononic stability of Janus single-layer MoSO. Before discussing the response of the vibrational spectrum to the applied biaxial strain, we first present our results for the electronic structure. As shown in Fig. 4, the semiconducting nature of Janus MoSO can be tuned via the application of biaxial strain. Mainly, two results can be obtained from the strain-dependent electronic band dispersions. One of our findings is that single-layer Janus

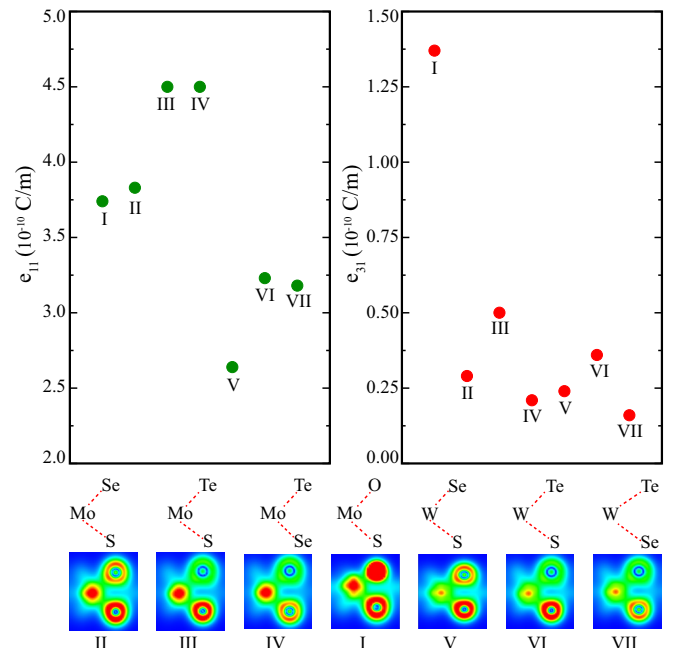


FIG. 3. The in-plane, e_{11} , and the out-of-plane, e_{31} , components of the piezoelectric stress coefficients of Janus MoSO, which are compared with the other predicted Janus TMDs. Side views of the charge differences on both surfaces are given below.

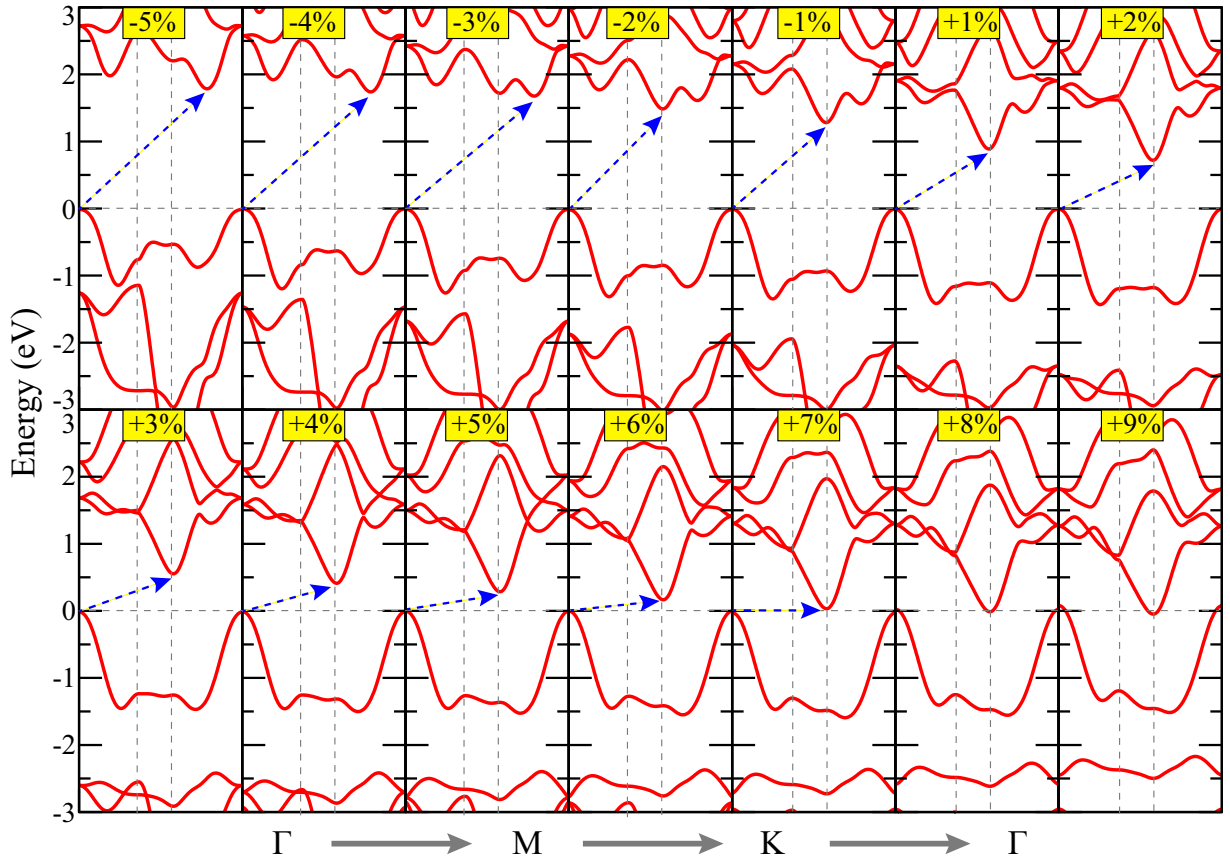


FIG. 4. In-plane biaxial strain-dependent electronic band dispersions of single-layer Janus MoSO. The Fermi level is set to zero energy.

MoSO undergoes a semiconducting-to-metallic transition for tensile strain over 8% ($\varepsilon > 8\%$) which is slightly smaller than that reported for single-layer MoS₂ (10%) [44]. We find a decreasing band gap via increasing tensile strain, while the band gap opens under application of compressive strain. Apparently, the conduction band edges are mostly affected by the applied in-plane biaxial strain. Therefore, as a result

of this, it is seen that the CBM of single-layer MoSO shifts from the K point to a point between K and Γ , which is the second main result of strain-driven electronic properties of MoSO. The CBM point crossover can also be seen in the graph presented in Fig. 5. Basically, the shift of the CBM can be related to the atomic orbital character of the CBM at the K point. As shown in Fig. 2, due to the out-of-plane character of the orbitals occupying the VBM, it is almost unaffected by the applied in-plane strain; however, due to the mixed d_{x^2} and d_{z^2} orbitals of the Mo atom at the CBM, it displays both a shift in position and an energy shift via applied strain.

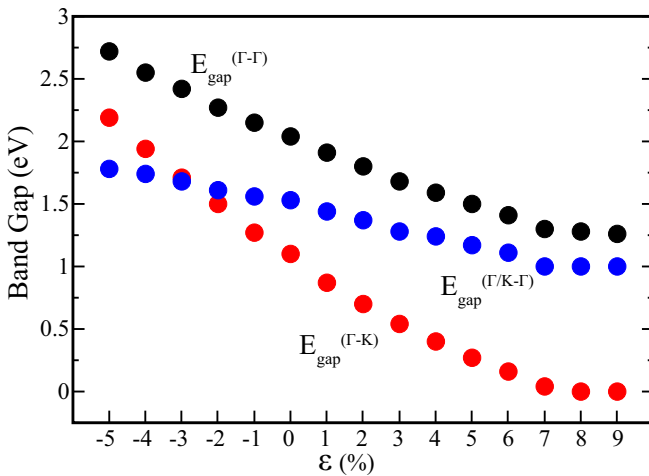


FIG. 5. The evolution of the direct and the indirect band gaps in single-layer MoSO under applied biaxial strain.

B. Phononic stability and Raman shifts

The stress-strain relation for a material can be used to extract its mechanical properties and also can be used to probe the elastic instability of the material at a certain applied strain. Many 2D materials undergo phononic instability before reaching the elastic instability. Therefore, in the case of single-layer Janus MoSO, we directly examine the strain-dependent phononic stability. As presented in Fig. 6, small imaginary frequencies around the Γ point increase for compressive strain of 5%. On the other hand, under the application of tensile strain, the structure retains its dynamical stability up to strain values of almost 12%. Notably, our reported critical strain value is smaller than those reported for graphene (15% for biaxial [45] and 18–24% for uniaxial strains [46]). In addition, the phononic instability strain value of MoS₂ (20%) [47,48] is

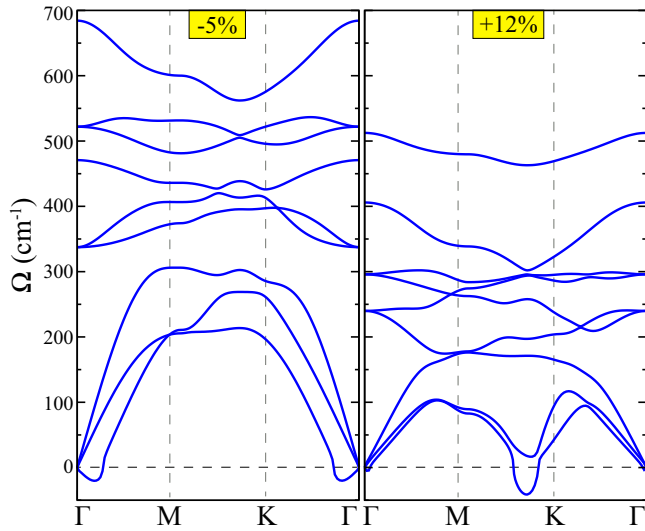


FIG. 6. Phonon band dispersions of 5% compressively (on the left) and 12% stretched biaxial strain (right) of single-layer MoSO. Imaginary frequencies are shown as negative frequencies.

much larger than our predicted value for single-layer Janus MoSO. At 12% of biaxial tensile strain, single-layer MoSO is found to undergo a phononic instability which is dictated by both out-of-plane and in-plane soft modes between the M and the K points. This is also known as the finite wave vector instability, which is expected to occur in 2D materials. Notably, in addition to the out-of-plane flexural acoustic mode, the in-plane acoustic mode also causes phononic instability, which can be attributed to the broken out-of-plane symmetry in the Janus structure. Here the underlying mechanism can be understood through the bonds Mo-O and Mo-S. As the applied tensile strain increases, the Mo-S and Mo-O bonds become more flat, which softens the out-of-plane and in-plane acoustic modes.

The investigation of phonon shifts and the variation of Raman activities of the Raman active modes can be useful to probe the strain on the material. As shown in Fig. 7(a), compressive (tensile) biaxial strain hardens (softens) the frequencies of both in-plane and out-of-plane phonon modes. However, as the applied biaxial strain is in-plane, the

responses of the phonon modes are not expected to be the same due to their different mode Grüneisen parameters.

The mode Grüneisen parameter for a phonon mode can be calculated using the relation

$$\gamma(q) = -\frac{a_0}{2\omega_0(q)} \left[\frac{\omega_+(q) - \omega_-(q)}{a_+ - a_-} \right], \quad (3)$$

where a_0 is the optimized lattice constant, $\omega_0(q)$ is the unstrained phonon frequency at wave vector q , $\omega_+(q)$ and $\omega_-(q)$ are the phonon frequencies under tensile and compressive biaxial strain, respectively, and $a_+ - a_-$ is the difference in the lattice constant when single-layer MoSO is under biaxial strain. In the present study, the phonon frequencies are calculated in the $q = 0$ limit, at the Γ point. As presented in Fig. 7(b), the frequency shifts of the phonon modes are different from each other due to their different vibrational characters. The calculated mode Grüneisen parameters for the E'' , A_1^S , E' , and A_1^O modes are 0.70, 0.26, 1.32, and 0.84, respectively. All of these values are larger as compared to fully symmetric single-layer TMDs (0.52, 0.68, and 0.23 for E'' , E' , and A_1 modes of single-layer MoS₂) [49]. All phonon modes are found to display phonon softening (hardening) via applied tensile (compressive) strains. This is a direct indication of the changing electron distribution or atomic bonding in the structure with strain. The phonon frequency shifts are important for probing the type and strength of the applied strain in the structure. As the A_1^S has the lowest mode Grüneisen parameter, the shift of its frequency is the smallest among all the phonon modes of MoSO. Therefore, it can be seen in Fig. 7(a) that the frequency of E' becomes smaller than that of A_1^S for tensile biaxial strain. Notably, vibrations of the phonon modes, E' and A_1^O , are dominated by the O atoms and thus the shifts of the two modes are larger with applied strain due to Mo-O bonds, which become more horizontal to the Mo layer.

We present our results up to strain value of 9%, at which semiconducting-metallic transition is driven for MoSO. The transition of single-layer MoSO from semiconducting to metallic significantly affects the Raman activities of the Raman active modes. Therefore, we separated our results for the tensile strains over 6%, after which the Raman activities become much larger due to the electronic contributions to the Raman activity. The Raman activities in the range of $\pm 5\%$ strain are multiplied by a factor of 200 in order to be comparable to those for strains over 6%. The Raman activity

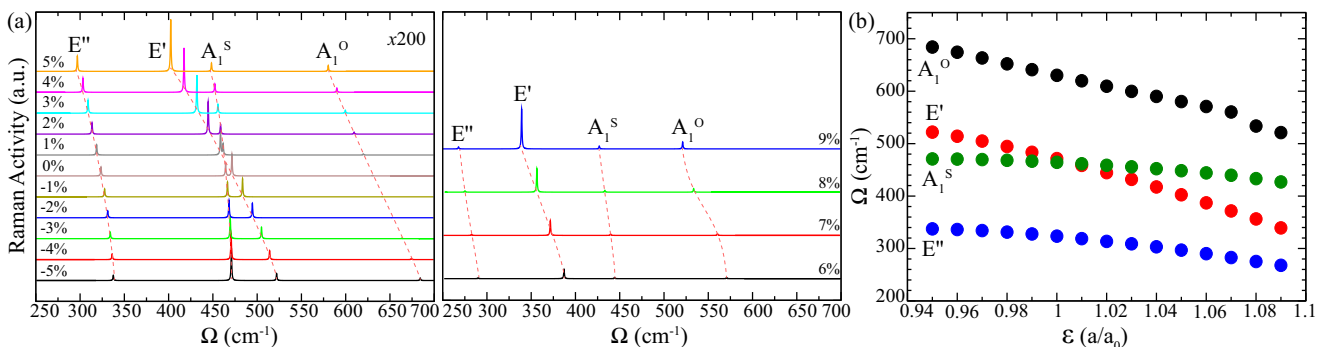


FIG. 7. (a) The evolution of the Raman spectrum of single-layer MoSO under compressive and tensile strains. (b) The strain-dependent phonon frequency shifts of the four Raman active modes.

of in-plane vibration modes E' and E'' , displays an increasing trend from compressive to tensile strain. Since the applied strain is in-plane, it rearranges the electron clouds between the Mo-S and Mo-O atoms which significantly enhances the polarizability and hence the Raman activity. This behavior is the same as that reported for fully symmetric single-layer TMDs under biaxial strain [49]. The A_1^O mode, which cannot be observed in symmetric single-layer TMDs, exhibits also an increasing trend in its Raman activity with increasing tensile strain. In fact this behavior is in contrast to what was reported for the A_1 mode of single-layer MX_2 ($M = \text{Mo}$ or W and $X = \text{S}$ or Se) [49]. The main difference between a TMD's single layer and the Janus structure arises from the different vibrational motion of the atoms. In fully symmetric TMDs, the A_1 mode represents the out-of-plane vibration of only the chalcogen atoms while in a Janus single layer this mode arises mainly from the out-of-plane vibration of a chalcogen and transition metal atoms. The direct bonding between the vibrating atoms in the Janus structure influences strongly the Raman activity response of the phonon mode against the applied strain. In contrast to the A_1^O mode, the other out-of-plane vibrational mode, A_1^S , possesses a decreasing trend in its Raman activity with increasing tensile strain, which is similar to that of symmetric single-layer TMDs [49]. Such behavior arises from the vibration of the chalcogen atoms dominating the phonon mode.

V. CONCLUSION

In this study, the 1H phase of a Janus single layer composed of S-Mo-O atomic layers was predicted to be dynamically stable and to be an indirect band gap semiconductor. Our findings revealed that the single-layer Janus structure of 1H-MoSO exhibits relatively strong polarization arising from the

large charge difference between S and O surfaces. In contrast to 1H phases of MoS_2 and MoO_2 , Janus MoSO was shown to possess four Raman active phonon modes in its Raman spectrum, which is a fingerprint for the observation of the Janus crystal. Among the 1H-phase Janus single-layer TMDs, single-layer MoSO was found to exhibit a much stronger out-of-plane piezoelectric coefficient. Moreover, we investigated the electronic and phononic properties of Janus MoSO under applied biaxial strain. Our results indicated the following: (i) single-layer MoSO undergoes a semiconducting-to-metallic phase transition via applied tensile strain while the conduction band edge displays a shift under compressive strain. (ii) single-layer MoSO preserves its phononic stability under applied 5% of compressive strain and 11% of tensile strain, displaying significant phonon shifts. (iii) Raman activity of the phonon modes was shown to display significant enhancement as the semiconducting-to-metallic transition is reached, which is due to the fact that the electronic transitions start to contribute to the Raman activity. In addition, the phonon instability was shown to arise from the soft in-plane and out-of-plane acoustic modes at finite wave vector. The large strain tolerance of Janus MoSO is important for its nanoelastic applications. With its strain-free and strain-dependent stability, we propose that Janus MoSO can be fabricated in the common 1H phase with a strong out-of-plane piezoelectric coefficient.

ACKNOWLEDGMENTS

Computational resources were provided by the Flemish Supercomputer Center (VSC). M.Y. is supported by the Flemish Science Foundation (FWO-VI) through a postdoctoral fellowship.

-
- [1] S. K. Novoselov, A. K. Geim, S. V. Morozov, D. Jiang, Y. Zhang, S. V. Dubonos, I. Grigorieva, and A. A. Firsov, *Science* **306**, 666 (2004).
- [2] A. H. Castro Neto and K. Novoselov, *Rep. Prog. Phys.* **74**, 082501 (2011).
- [3] K. F. Mak, C. Lee, J. Hone, J. Shan, and T. F. Heinz, *Phys. Rev. Lett.* **105**, 136805 (2010).
- [4] A. Splendiani, L. Sun, Y. Zhang, T. Li, J. Kim, C.-Y. Chim, G. Galli, and F. Wang, *Nano Lett.* **10**, 1271 (2010).
- [5] B. Radisavljevic, A. Radenovic, J. Brivio, I. V. Giacometti, and A. Kis, *Nat. Nanotechnol.* **6**, 147 (2011).
- [6] J. T. Ye, Y. J. Zhang, R. Akashi, M. S. Bahramy, R. Arita, and Y. Iwasa, *Science* **338**, 1193 (2012).
- [7] R. V. Kasowski, *Phys. Rev. Lett.* **30**, 1175 (1973).
- [8] L. F. Mattheis, *Phys. Rev. Lett.* **30**, 784 (1973).
- [9] L. F. Mattheis, *Phys. Rev. B* **8**, 3719 (1973).
- [10] S. Lebegue and O. Eriksson, *Phys. Rev. B* **79**, 115409 (2009).
- [11] H. S. S. Ramakrishna Matte, A. Gomathi, A. K. Manna, D. J. Late, R. Datta, S. K. Pati, and C. N. R. Rao, *Angew. Chem.* **122**, 4153 (2010).
- [12] K. Liu, Q. Yan, M. Chen, W. Fan, Y. Sun, J. Suh, D. Fu, S. Lee, J. Zhou, S. Tongay, J. Ji, J. B. Neaton, and J. Wu, *Nano Lett.* **14**, 5097 (2014).
- [13] J. Zhou, J. Lin, X. Huang, Y. Zhou, Y. Chen, J. Xia, H. Wang, Y. Xie, H. Yu, J. Lei, D. Wu, F. Liu, Q. Fu, Q. Zeng, C.-H. Hsu, C. Yang, L. Lu, T. Yu, Z. Shen, H. Lin, B. I. Yakobson, Q. Liu, K. Suenaga, G. Liu, and Z. Liu, *Nature (London)* **556**, 355 (2018).
- [14] V. Senthilkumar, L. C. Tam, Y. S. Kim, Y. Sim, M. J. Seong, and J. I. Jang, *Nano Res.* **7**, 1759 (2014).
- [15] Y.-F. Lim, K. Priyadarshi, F. Bussolotti, P. K. Gogoi, X. Cui, M. Yang, J. Pan, S. W. Tong, S. Wang, S. J. Pennycook, K. E. J. Goh, A. T. S. Wee, S. L. Wong, and D. Chi, *Phys. Rev. B* **92**, 085427 (2015).
- [16] X. L. Li and Y. D. Li, *Chem. Eur. J.* **9**, 2726 (2003).
- [17] P. Arnoldy, J. A. M. van den Heijkant, G. D. De Bok, and J. A. Moulijn, *J. Catal.* **92**, 35 (1985).
- [18] Y. Okamoto, A. Kato, Usman, N. Rinaldi, T. Fujikawa, H. Koshika, I. Hiromitsu, and T. Kubota, *J. Catal.* **265**, 216 (2009).
- [19] Z. Wu, D. Wang, and A. Sun, *J. Cryst. Growth* **312**, 340 (2010).
- [20] A.-Y. Lu, H. Zhu, J. Xiao, C.-P. Chuu, Y. Han, M.-H. Chiu, C.-C. Cheng, C.-W. Yang, K.-H. Wei, Y. Yang, Y. Wang, D. Sokaras, D. Nordlund, P. Yang, D. A. Muller, M.-Y. Chou, X. Zhang, and L.-J. Li, *Nat. Nanotechnol.* **12**, 744 (2017).
- [21] J. Zhang, S. Jia, I. Kholmanov, L. Dong, D. Er, W. Chen, H. Guo, Z. Jin, V. B. Shenoy, L. Shi, and J. Lou, *ACS Nano* **11**, 8192 (2017).

- [22] A. Kandemir and H. Sahin, *Phys. Rev. B* **97**, 155410 (2018).
- [23] Y. C. Cheng, Z. Y. Zhu, M. Tahir, and U. Schwingenschlögl, *Europhys. Lett.* **102**, 57001 (2013).
- [24] L. Dong, J. Lou, and V. B. Shenoy, *ACS Nano* **11**, 8242 (2017).
- [25] M. Yagmurcukardes, C. Sevik, and F. M. Peeters, *Phys. Rev. B* **100**, 045415 (2019).
- [26] Z. Kahraman, A. Kandemir, M. Yagmurcukardes, and H. Sahin, *J. Phys. Chem. C* **123**, 4549 (2019).
- [27] J. P. Perdew, K. Burke, and M. Ernzerhof, *Phys. Rev. Lett.* **77**, 3865 (1996).
- [28] J. P. Perdew, K. Burke, and M. Ernzerhof, *Phys. Rev. Lett.* **78**, 1396 (1997).
- [29] G. Kresse and J. Hafner, *Phys. Rev. B* **47**, 558 (1993).
- [30] G. Kresse and J. Hafner, *Phys. Rev. B* **49**, 14251 (1994).
- [31] J. Heyd, G. E. Scuseria, and M. Ernzerhof, *J. Chem. Phys.* **118**, 8207 (2003).
- [32] S. J. Grimme, *Comput. Chem.* **27**, 1787 (2006).
- [33] G. Henkelman, A. Arnaldsson, and H. Jonsson, *Comput. Mater. Sci.* **36**, 354 (2006).
- [34] D. Alfe, *Comput. Phys. Commun.* **180**, 2622 (2009).
- [35] See Supplemental Material at <http://link.aps.org/supplemental/10.1103/PhysRevB.101.155205> for electronic band dispersions of single-layers of MoS₂ and MoO₂. The thermal stability of 1H-MoSO and the phonon band dispersions of the 1T phase of Janus MoSO are also presented.
- [36] M. N. Blonsky, H. L. Zhuang, A. K. Singh, and R. G. Hennig, *ACS Nano* **9**, 9885 (2015).
- [37] M. M. Alyoruk, Y. Aierken, D. Cakir F. M. Peeters, and C. Sevik, *J. Phys. Chem. C* **119**, 23231 (2015).
- [38] R. Fei, W. Li, and J. Li, *Appl. Phys. Lett.* **107**, 173104 (2015).
- [39] L. C. Gomes, A. Carvalho, and A. H. Castro Neto, *Phys. Rev. B* **92**, 214103 (2015).
- [40] F. Guinea, M. I. Katsnelson, and A. K. Geim, *Nat. Phys.* **6**, 30 (2009).
- [41] K. He, C. Poole, K. F. Mak, and J. Shan, *Nano Lett.* **13**, 2931 (2013).
- [42] Z. H. Ni, T. Yu, Y. H. Lu, Y. Y. Wang, Y. P. Feng, and Z. X. Shen, *ACS Nano* **2**, 2301 (2008).
- [43] M. Huang, H. Yan, T. F. Heinz, and J. Hone, *Nano Lett.* **10**, 4074 (2010).
- [44] E. Scalise, M. Houssa, G. Pourtois, V. Afanasev, and A. Stesmans, *Nano Res.* **5**, 43 (2012).
- [45] F. Liu, P. Ming, and J. Li, *Phys. Rev. B* **76**, 064120 (2007).
- [46] C. A. Marianetti and H. G. Yevick, *Phys. Rev. Lett.* **105**, 245502 (2010).
- [47] T. Li, *Phys. Rev. B* **85**, 235407 (2012).
- [48] E. B. Isaacs and C. A. Marianetti, *Phys. Rev. B* **89**, 184111 (2014).
- [49] M. Yagmurcukardes, C. Bacaksiz, E. Unsal, B. Akbali, R. T. Senger, and H. Sahin, *Phys. Rev. B* **97**, 115427 (2018).